Evaluation of Theoretical CFV Flow Models in the Laminar, Turbulent, and Transition Flow Regimes

By Aaron Johnson and John Wright
NIST
100 Bureau Drive Mail stop 8361
Gaithersburg, MD 20899
Phone: 301-975-5954, Fax: 301-258-9201, aaron.johnson@nist.gov, john.wright@nist.gov

ABSTRACT
State of the art dimensional metrology was used to measure the throat diameter and throat curvature of nine critical flow venturis (CFVs) with nominal throat diameters ranging from 5 mm to 25 mm. The throat curvature was used calculate the theoretical discharge coefficients while the throat diameter was used to compute the experimental discharge coefficients. The nine CFVs were calibrated in dry air using two NIST primary flow standards with expanded uncertainties of 0.05 % and 0.09 %, respectively. The calibration data spans a Reynolds number range from 7.2×10^4 to 2.5×10^6, including laminar, turbulent, and transition flow regimes. By correcting for both the throat diameter and curvature, the agreement between predicted and measured discharge coefficients was less than 0.17 % in the turbulent regime and less than 0.07 % in the laminar regime.

1. INTRODUCTION

Critical flow venturis (CFVs) are widely used in the flow metering community as flow meters, check standards, and transfer standards. The popularity of these devices is a result of their excellent long term reproducibility [1], simple geometric design [2], straightforward application, and well understood physics. Much of the pioneering work for CFV flow meters was done during the 1960's and 1970's when numerous theoretical flow models were developed for predicting the CFV discharge coefficient.

Recent calibration data taken in air by Ishibashi [3] quantified the accuracy of these models over a portion of the laminar flow regime. Ishibashi's measurements of the discharge coefficient agreed with theoretical predictions to better than 0.03 % over a Reynolds numbers range extending from 8×10^4 to 2.5×10^5. For this comparison he used *high precision nozzles* (HPNs), manufactured on ultra high precision lathes, whose throat diameters (d) are known to better than a fraction of a micron, and whose throat radius of curvature (r_c) and overall CFV profiles match the ISO [2] recommended shape extremely well, generally within 1 μm. This makes HPNs an excellent choice for comparing measured versus predicted values of the discharge coefficient.

Unfortunately for CFV theorists, the cost of an HPN is approximately ten times that of a "normally manufactured" CFV and therefore they are not widely used by the flow metering community. By "normally manufactured", we mean produced on something less than an ultra high precision lathe and generally polished after machining. For practical reasons, it is of interest to determine how well the discharge coefficients of normally manufactured CFVs compare with theoretically predicted values.

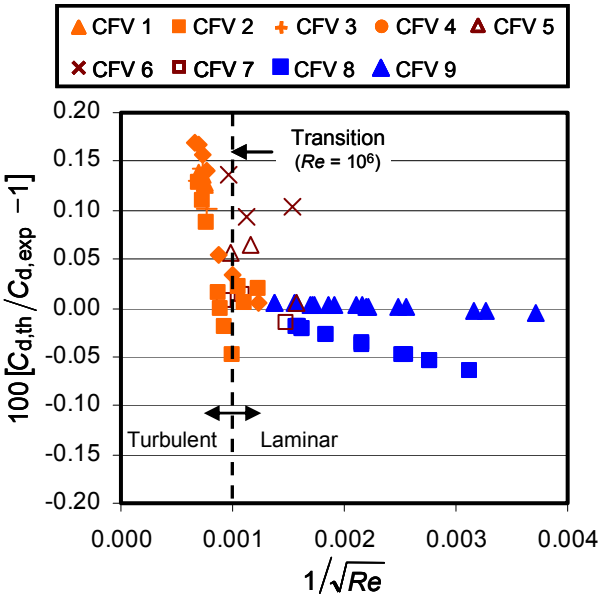

Figure 1. *Percent Difference between theoretical models and experimental data for nine normally manufactured CFVs.*

In this work, we measured both the throat diameter (d) and the throat curvature ratio ($\Omega \equiv d/2r_c$) of nine normally manufactured CFVs using NIST's Moore M48 coordinate measurement machine (CMM) [4]. The measured d's were used in calculating the experimental discharge coefficients ($C_{d,exp}$) while Ω's were used in calculating the predicted discharge coefficients ($C_{d,th}$). Figure 1 shows the overall agreement between $C_{d,exp}$ and $C_{d,th}$ is better than 0.17 % over a Reynolds number range extending from 7.2×10^4 to 2.5×10^6. This good agreement is surprising since no effort was made to account for boundary layer transition from laminar to turbulent flow. Instead, we implemented a simple piecewise model that assumed laminar flow for Reynolds numbers below 10^6 and turbulent flow at higher Reynolds numbers.

This paper presents the results of the comparisons between $C_{d,th}$ and $C_{d,exp}$, describes the NIST flow standards used to measure the CFV discharge coefficients, describes the dimensional CFV measurements, and reviews the theoretical models used to predict the discharge coefficient.

2.1 FLOW STANDARDS AND THE HISTORICAL CALIBRATION RECORDS OF CFVs

The nine CFVs were calibrated using two *PVTt* flow standards with nominal collection volumes of 677 L and 26 m^3 respectively. Jointly these *PVTt* systems cover a flow range extending from 100 L/min to 78000 L/min.[1] The two smallest CFVs were calibrated using both the 677 L *PVTt* flow standard and the 26 m^3 *PVTt* flow standard. The remaining seven CFVs were calibrated only on the 26 m^3 *PVTt* standard. For all of the calibrations the CFV stagnation temperature was maintained close to room temperature while the stagnation pressure ranged from 150 kPa to 850 kPa. The expanded mass flow uncertainties for the 677 L and 26 m^3 *PVTt* systems are 0.05 % [5] and 0.09 % [6, 7], respectively.

Table 1 shows the calibration history for the set of nine CFVs. For convenience, each CFV is identified throughout this document by the numerical value in column one. The remaining columns list the total number of calibration points (where the number of calibrations are in parenthesis), the standard deviation of residuals between a best fit curve of all the calibration data and the measured discharge coefficients, and the relative uncertainty of the measured discharge coefficients (where the values in parenthesis are the uncertainties obtained on the 677 L *PVTt* standard). In its entirety, the calibration records contain 1007 data points.

Table 1. *Calibration history for selected CFVs using dry air as the working fluid.*

CFV No.	No. of Points (No. Cals.)	Std. Dev. of Best Fit Residuals	Rel. Unc. of $C_{d,exp}$ (k = 2)
( )	( )	($\times 10^6$)	(%)
1	37 (1)	80	0.11
2	79 (1)	170	0.11
3	42 (1)	137	0.11
4	62 (1)	68	0.11
5	150 (3)	405	0.11
6	60 (2)	482	0.21
7	90 (3)	460	0.11
8	234 (4)	300	0.11 (0.08)
9	253 (4)	290	0.11 (0.08)

The largest source of uncertainty of $C_{d,exp}$ stems from the *PVTt* mass flow measurements. Other factors including the stagnation pressure, stagnation temperature, critical flow factor, CFV throat diameter, etc. also contribute, increasing the uncertainty of $C_{d,exp}$ slightly above the uncertainty of mass flow. The uncertainty of CFV 6 is larger than its counterparts since all of its calibration data precedes 2003, when performance upgrades to the 26 m^3 *PVTt* flow standard reduced its uncertainty from 0.21 % to 0.09 % [6, 7, 8]. This larger uncertainty is believed to be responsible for the results in Fig. 1 where the difference between theory and experiment in the laminar flow range is larger for CFV 6 than for the other CFVs.

2.2 DIMENSIONAL CFV MEASUREMENTS

The throat diameter (d) and the throat curvature ratio (Ω) are the key geometric parameters for comparing $C_{d,exp}$ to $C_{d,th}$. Highly accurate values of d (*i.e.*, better than 0.05 % with k = 2) are required to ensure low uncertainty $C_{d,exp}$ values. On the other hand, $C_{d,th}$ is not as sensitive to Ω so that relatively large uncertainties can be

[1] Unless otherwise noted all volumetric flows in this paper are taken to be at standard conditions with a temperature at 293.15 K and a pressure of 101.325 kPa.

tolerated. For the Reynolds number range considered in this paper, an uncertainty of 10 % or less is acceptable, affecting the predicted discharge coefficient by no more than 0.03 %.

The Moore M48 CMM is used to determine both d and Ω by measuring (r, θ) data around the circumference of various cross sections passing through the CFV throat. Here, r is the radius measured from the CFV centerline and θ is the angle for a polar coordinate system. At each cross section, we measured twelve radial measurements spaced 30 degrees apart. These twelve measurements are used to calculate the cross sectional area. In this work the cross sectional area is estimated by fitting the *best fit* ellipse through the twelve points. The ellipsoidal fit accounts for eccentricity observed in some of the CFVs, but collapses to a circle in the special case where the data is perfectly round. By dividing the ellipsoidal area by π, and taking its square-root we determine the *effective* radius at each cross section. The average CFV contour was estimated by fitting the measured data to either a fifth or sixth degree polynomial of the effective radius as a function of axial position. The axial position of the throat is determined by setting the derivative of the polynomial equal to zero. The throat diameter equals twice the value of the polynomial evaluated at the axial throat location, and the throat curvature equals the second derivative of the polynomial evaluated at the throat location.

Table 2 shows the throat diameter, the throat curvature ratio, and their expanded relative uncertainties (*i.e.*, $k = 2$) for all nine CFVs. The table shows that the measured Ω ranged from 0.11 to 0.28. This range of values was surprising since all nine CFVs were manufactured to comply with ISO specifications. For an ISO manufactured CFV, Ω should have a value between 0.227 and 0.278. Only CFVs 5 and 6 satisfy this criterion. For CFVs 8 and 9 the difference between the optimum ISO curvature ratio (selected to be $\Omega_{ISO} = 0.25$ in this work) and the measured values are more than 100 %. This large difference would have introduced significant error in predicting the discharge coefficient had we not measured Ω.

In Table 2, the uncertainties of the throat diameters are calculated by root-sum-squaring the 0.5 μm ($k = 1$) uncertainty from the CMM measurements and the uncertainty attributed to eccentricity (*i.e.*, departure from circularity) of the CFV cross section. The standard uncertainty attributed to eccentricity is taken to be proportional to the absolute difference of two throat radii. Each radius is calculated by square-rooting the throat cross sectional area divided by π; however, two different methods are used to obtain the cross sectional area. In one case, the best fit ellipse (as explained previously) is used to determine the throat cross sectional area while in the other case the best fit circle is used. Since we expect the uncertainty to fall between these two radii, a rectangular distribution is assumed and the standard uncertainty is taken equal to the absolute difference of the two radii divided by $\sqrt{3}$ [9].

Table 2. *Measured values of throat diameter (d) and curvature ratio (Ω) and their relative uncertainties ($k = 2$).*

CFV No. ( )	d (mm)	$\left[\frac{u(d)}{d}\right]$ (%)	Ω ( )	$\left[\frac{u(\Omega)}{\Omega}\right]$ (%)
1	25.3932	0.004	0.186	6.0
2	25.39098	0.004	0.192	8.1
3	25.3935	0.004	0.204	8.4
4	25.3883	0.004	0.18	7.4
5	19.7517	0.005	0.26	1.6
6	18.7857	0.005	0.265	2.9
7	17.3489	0.006	0.28	2.4
8	6.3784	0.020	0.12	51.7
9	4.8284	0.021	0.11	9.4

The uncertainty of the throat curvature ratio is taken equal to the standard deviation of twelve values of Ω, each calculated along one of the twelve CFV contours spaced 30°degrees apart.[2] The value of $[u(\Omega)/\Omega]$ is affected by the degree of eccentricity of the cross sectional shape of the CFV. If the cross sectional shape is nearly circular, than the values of Ω will be nearly constant along the throat circumference, leading to the lower values of uncertainty in Table 2. Conversely, if the cross sectional shape is more ellipsoidal than circular, Ω will change substantially at different θ along the throat circumference, leading to the larger values of uncertainty. The cross sectional shape of CFV 8 had by far the largest departure from circularity, resulting in $[u(\Omega_8)/\Omega_8]$ being more than five times the next largest value. Moreover, this large

[2] Other sources of uncertainty are negligible.

uncertainty decreases the accuracy of the predicted discharge coefficient.

2.3 CFV PRINCIPLE OF OPERATION AND PHYSICS

Figure 2 shows an axisymmetric cut of a toroidal shaped CFV with dimensions complying with ISO 9300 standard [2]. The CFV profile consists of a circular arc extending slightly beyond the throat cross section to a point of tangency, followed by a conical divergent section with a half angle between 2 and 6 degrees. When sufficient pressure ratios (*i.e.*, P_b/P_0) exist across the CFV, the gas flow achieves sonic velocity near the throat. Here, P_0 is the upstream stagnation pressure and P_b is the static pressure downstream of the CFV exit. The largest pressure ratio that satisfies this condition is called the *choking pressure ratio* (CPR) and CFVs are operated at or below this value.

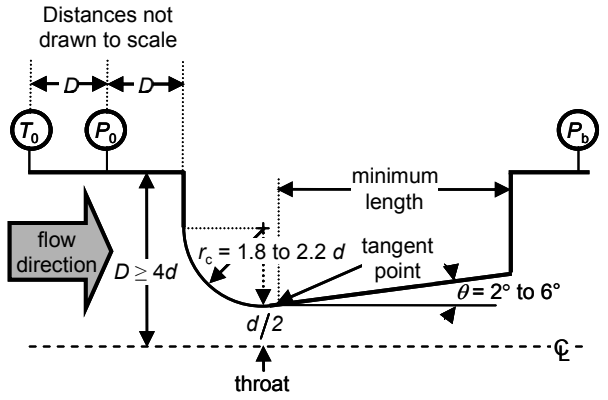

***Figure 2**. Axisymmetric cut of a toroidal shaped CFV with dimension specifications of the ISO 9300 standard [2].*

Under choked flow conditions (*i.e.*, P_b/P_0 less than the CPR) the CFV mass flow is independent of the thermodynamic conditions downstream of the throat section. Physically, pressure fluctuations cannot propagate upstream of the sonic throat.[3] Consequently, the mass flow is proportional to the upstream stagnation pressure alone, instead of the upstream to downstream pressure difference as in the case of a venturi operating at subsonic conditions.

Quantitative predictions of the CFV mass flow are commonly obtained via the published theoretical models [10-20]. The complexity as well as the accuracy of these models can vary significantly. The simplest of these models provides a common basis for all of the more sophisticated models and is herein called the *baseline* model. The baseline model is derived by reducing the Navier-Stokes equations [21] using the following three assumptions:

1) the flow is one-dimensional,
2) the flow processes are isentropic, and
3) the fluid is taken to be a calorically perfect gas (*i.e.*, C_p = constant).

Together, assumptions 1 through 3 are herein called the *sonic assumption*. Under the sonic assumption the baseline CFV mass flow is [10]

$$\dot{m}_b = \frac{\pi d^2 P_0 C_i^* \sqrt{\mathcal{M}}}{4\sqrt{R_u T_0}} \qquad (1)$$

where P_0 is the upstream stagnation pressure; T_0 is the upstream stagnation temperature; R_u is the universal gas constant, $\mathcal{M}$ is the molecular weight, and C_i^* is the *ideal* gas critical flow function

$$C_i^* = \sqrt{\gamma}\left[\frac{\gamma+1}{2}\right]^{\frac{\gamma+1}{2(1-\gamma)}} \qquad (2)$$

where $\gamma = C_p/C_v$ is the specific heat ratio evaluated at the upstream static pressure and temperature.

The sonic assumption typically leads to predicted mass flows that agree with measurements to much better than 5 % of the actual value (depending primarily on Reynolds number). However, the sonic assumption is not fully satisfied in actual CFV flows for the following three reasons:

1) The Boundary Layer: The isentropic assumption is not valid in the boundary layer adjacent to the CFV wall. In this region, viscous effects retard the fluid motion thereby reducing the gas velocity below the sonic velocity. Simultaneously, shear between adjacent fluid layers heat the gas, leading to larger temperatures, and subsequently lower densities than the fluid density in the inviscid core beyond the boundary layer. Together, the lower velocity and lower density lead to decreased mass flow through the boundary layer region than would be predicted by the baseline model.

2) The Inviscid Core: The flow in the center, beyond the boundary layers is multidimensional so

[3] In small CFVs the mass flow could exhibit some dependence on P_b attributed to pressure disturbances propagating upstream via the subsonic boundary layer.

that the profile of the sonic line (*i.e.*, locus of points where the Mach number is unity) is nearly parabolic instead of the flat profile predicted by the baseline model. The effect of the curved sonic line is to reduce the mass flow in the core region below the baseline model.

3) Virial Effects: Real gas effects alter both the sound speed and the density, causing them to differ from the values predicted for a perfect gas with a constant heat capacity. In this case, virial effects can either increase or decrease the CFV mass flow depending on the upstream stagnation conditions and gas specie.

Over the past 40 years, researchers have analyzed these three phenomena and developed corrections to the baseline model that we will compare to our experimental calibration data. For these comparisons the working fluid (*i.e.*, dry air) behaves nearly ideally so that virial effects can be neglected. Moreover, other phenomena, notably vibrational relaxation [22] and heat transfer from the CFV wall, can be significant in special cases, but are also negligible herein. Therefore, deviations in mass flow from $\dot{m}_b$ are caused primarily by boundary layer and inviscid core effects.

When virial effects are neglected, the baseline mass flow is used as the normalizing parameter in the definition of the discharge coefficient

$$C_d \equiv \frac{\dot{m}}{\dot{m}_b} = \frac{4\dot{m}\sqrt{R_u T_0}}{\pi d^2 P_0 C_i^* \sqrt{\mathcal{M}}} \qquad (3)$$

where $\dot{m}$ is either measured or determined theoretically. In general, the discharge coefficient is a function of several variables including the Reynolds number, the specific heat ratio, heat transfer effects at the CFV wall, etc. A complete list of all of the pertinent dimensionless parameters charactering the discharge coefficient is given in reference [23]. However, among the numerous parameters influencing the discharge coefficient, the Reynolds number is usually the most important. This fact has been demonstrated by numerous calibration data and by the various theoretical models. In this paper we use the following Reynolds number definition

$$Re = \frac{4\dot{m}_b}{\pi d \mu_0} \qquad (4)$$

where μ_0 is the molecular viscosity evaluated at the upstream stagnation conditions.

2.4 REVIEW OF EXISTING THEORETICAL MODELS

Although numerous theoretical models have been formulated to predict the discharge coefficient, no single model has been developed that simultaneously eliminates all three conditions of the sonic assumption. Instead, three distinct types of theoretical models have been developed, each focusing on improving a single aspect of the sonic assumption. This has resulted in three distinct definitions of theoretical discharge coefficients including

1) the viscous discharge coefficient, $C_{d,1}$
2) the inviscid discharge coefficient, $C_{d,2}$
3) and, the virial discharge coefficient, $C_{d,3}$

which are herein distinguished by the subscripts 1, 2, and 3 respectively. Each of these three discharge coefficients results from a different simplification of the Navier-Stokes equations. In particular, $C_{d,1}$ is derived by retaining conditions 2 and 3 of the sonic assumption, but modifying condition 1 to account for the boundary layer development along the CFV wall. In a similar manner, $C_{d,2}$ (or $C_{d,3}$) modifies the second (or third) condition of the sonic assumption while enforcing the remaining two. In this work, the gas behaves nearly ideally so that only models for $C_{d,1}$ and $C_{d,2}$ are discussed.

The Viscous Discharge Coefficient, $C_{d,1}$

The viscous discharge coefficient accounts for the boundary layer development along the CFV wall. Predictive models have been developed both for laminar [11, 12] and for turbulent flows [13]. For a smooth CFV contour, boundary layer transition from laminar to turbulent flow typically occurs within a Reynolds number range extending from 8×10^5 to 1.2×10^6. Transition, however, has been observed at significantly lower Reynolds numbers in CFVs with rough walls. In this work all of the CFVs have sufficiently smooth walls so that transition to turbulent flow occurs within the normal Reynolds number regime.

Among the various laminar flow models the two most sophisticated and accurate models were developed independently by Tang in 1969 and by Geropp in 1971. Both of these models used similarity transformations to solve the axisymmetric compressible boundary layer equations. The turbulent flow model was developed in 1964 by Stratford who used an integral boundary layer technique to determine the turbulent displacement thickness, and subsequently the viscous discharge

coefficient. For either laminar or turbulent flow the viscous discharge coefficient has the following form

$$C_{d,1} = 1 - a_1 \Omega^{-m} Re^{-n} + a_2 \Omega^{-2m} Re^{-2n} \qquad (6)$$

where a_1 and a_2 are coefficients, and m and n are exponents whose values depend on whether the flow is laminar or turbulent. Table 3 gives the values of these coefficients and exponents for the various models. The viscosity ratio (μ^*/μ_0) in both Tang's and Stratford's model convert between the Reynolds number definition based on the stagnation molecular viscosity (μ_0) given in Eqn. 5 and the Reynolds number based on the molecular viscosity evaluated at the CFV throat (μ^*) that was used in these models. If the viscosity ratio in Tang's model is calculated assuming a simple linear relationship between viscosity and temperature (*i.e.*, $\mu = \lambda T$ where λ is a constant) then $a_{1,\text{Tang}} = a_{1,\text{Geropp}}$. In this work, however, we calculated μ^*/μ_0 using Sutherland's viscosity-law [21]. We hoped that using a more accurate viscosity model would improve the accuracy of $C_{d,1}$ predictions, but the comparisons to measured data did not support this approach. The reasoning is probably because the Sutherland model is not consistent with the linear relationship between viscosity and temperature used in the derivation of Tang's model.

The coefficients a_1 and a_2 were calculated using a nominal value of the specific heat ratio for dry air (γ = 1.405). No attempt was made to account for the slight variation in $\gamma(P,T)$ attributed to different CFV operating conditions (*i.e.*, different pressures and temperatures at the CFV inlet). The change in $C_{d,1}$ attributed to the slight variation in γ was less than 0.006 % and taken to be negligible for the range of Reynolds numbers considered in this work.

For laminar CFV flows with Reynolds number larger than 10^4, the last term in Eqn. 6 is small relative to the other terms and is often omitted. For example, for the Reynolds number range considered in this paper, this term accounts for less than 0.005 % of $C_{d,1}$. Consequently, the measured discharge coefficient scales almost linearly with $1/\sqrt{Re}$.

The largest difference between Tang's laminar boundary layer model with Geropp's model occurred at the lowest Reynolds number (*i.e.*, 7.2×10^4) and was only 0.028 %. At the higher Reynolds numbers the difference monotonically decreased. Between these two models, Geropp's boundary layer model agreed better with measured results and was therefore used for the comparison.

Table 3. *Coefficients, exponents, for selected boundary layer models used for predicting* $C_{d,1}$.

Viscous Solutions for $C_{d,1}$	Flow Type	Exponents		Coefficients	
		m	n	a_1	a_2
Tang, 1969 [11]	Laminar	1/4	1/2	$2\left[\frac{\gamma\sqrt{2}+6\sqrt{3}-7\sqrt{2}}{\sqrt{3}}\right]\left(\frac{\gamma+1}{2}\right)^{-1/4}\left(\frac{\mu^*}{\mu_0}\right)^{1/2}$	$\left[\frac{2\sqrt{2}}{3}\frac{(\gamma-1)(\gamma+2)}{\sqrt{\gamma+1}}\right]\left(\frac{\mu^*}{\mu_0}\right)$
Geropp, 1971 [12]	Laminar	1/4	1/2	$2\left[\frac{\gamma\sqrt{2}+6\sqrt{3}-7\sqrt{2}}{\sqrt{3}}\right]\left(\frac{\gamma+1}{2}\right)^{-3/4}$	$\left[\frac{\gamma\sqrt{2}+6\sqrt{3}-7\sqrt{2}}{\sqrt{3}}\right]^2\left(\frac{\gamma+1}{2}\right)^{-3/2}$
Stratford,[4] 1964 [13]	Turbulent	2/5	1/5	$\left(\frac{21}{400}\right)\left(\frac{1}{2}\right)^{2/5}\left(\frac{\mu^*}{\mu_0}\right)^{1/5}$	0

[4] This model was derived assuming the specific heat ratio Equals γ = 1.4.

Table 4. *Coefficients and expansion parameter for various series solutions of* $C_{d,2}$.

Inviscid Discharge Coefficient $C_{d,2}$	**Series Expansion Parameter** Λ	**Series Expansion Coefficients** α_2	α_3	α_4
Original Hall, 1962 [14]	R	$\frac{\gamma+1}{96}$	$\frac{(\gamma+1)(8\gamma+21)}{4608}$	$\frac{(\gamma+1)(754\gamma^2+1971\gamma+2007)}{552960}$
Corrected Hall, 1969 [15]	R	$\frac{\gamma+1}{96}$	$\frac{(\gamma+1)(8\gamma+21)}{2304}$	$\frac{(\gamma+1)(754\gamma^2+2123\gamma+2553)}{552960}$
Kliegel and Levine, 1969 [15]	$1+R$	$\frac{\gamma+1}{96}$	$\frac{(\gamma+1)(8\gamma-27)}{2304}$	$\frac{(\gamma+1)(754\gamma^2-757\gamma+3633)}{276480}$

The Inviscid Discharge Coefficient, $C_{d,2}$

Several researchers [13-15] have developed methods for determining the inviscid discharge coefficient. Perhaps, the most widely used model was developed by Hall in 1962. Hall assumed that the gas behaved ideally and had a constant heat capacity. He used a perturbation series expansion in powers of $1/R$ (where $R = 1/\Omega$) to solve the steady, irrotational, axisymmetric, compressible flow equation in the transonic regime [14]. Since the series diverges for $R < 1$, it is not unexpected that the accuracy of this solution diminishes for small values of R. In fact, for sufficiently small R, Hall's solution yields non-physical results, predicting negative values of the inviscid discharge coefficient. Consequently, the common practice has been to avoid using this solution for $R < 2$. In 1969, Kliegel and Levine extended and improved Hall's work by using a perturbation series solution expanded about $1/(1+R)$ that converges for all values of R. In developing the improved series solution, Kliegel and Levine found an error in Hall's original solution and provided the appropriate correction

The mathematical formulation of the inviscid discharge coefficient is

$$C_{d,2} = 1 - \frac{\alpha_2}{\Lambda^2} + \frac{\alpha_3}{\Lambda^3} - \frac{\alpha_4}{\Lambda^4} \qquad (7)$$

where α_2, α_3, and α_4 are species dependent coefficients and Λ is the expansion parameter. Table 4 gives the values of the coefficients and the expansion parameters for Hall's original solution, the corrected version of Hall's solution, and the improved solution of Kliegel and Levine. Figure 3 compares the predicted discharge coefficients given by these three models versus Ω for γ = 1.405. The left y-axis gives the values of $C_{d,2}$ for each of the three models while the right y-axis gives the percent difference between the original series solution of Hall and the improved series solution of Kliegel and Levine. Within the ISO specified design limits (indicated by the shaded rectangle) the difference between these two solutions is no more than 0.03 %, but increases to as much as 0.2 % for Ω = 0.5 (R = 2) with the difference increasing further at larger Ω (or smaller R).

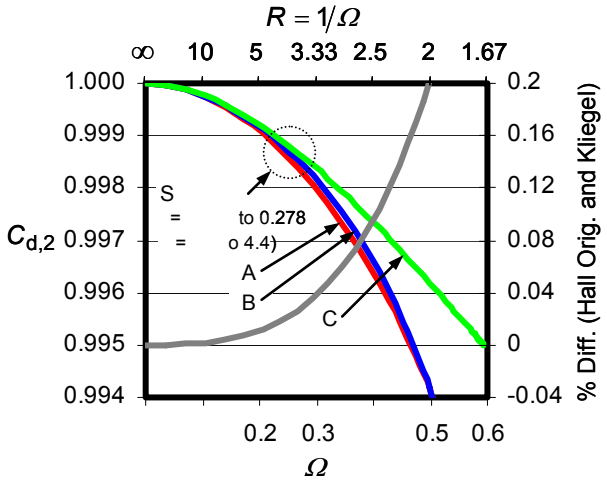

Figure 3*. Comparison of three models of the inviscid discharge coefficient. (A – original solution of Hall [14], B – corrected version of Hall's solution [15], and C – solution of Kliegel and Levine [15])*

Combining $C_{d,1}$ and $C_{d,2}$ to Predict the Measured Discharge Coefficient

Throughout the years, researchers have approximated the measured discharge coefficient by combining $C_{d,1}$ and $C_{d,2}$ as either a linear combination [13]

$$C_{d,th} = C_{d,1} + C_{d,2} - 1 \qquad (8a)$$

or as a simple product [20]

$$C_{d,th} = C_{d,1}\, C_{d,2} \qquad (8b)$$

of the two theoretical discharge coefficients.[5] A common shortcoming of both methods is that neither accounts for coupling effects between the boundary layer and inviscid core which could play a role for CFVs with large Ω operating at low Reynolds. In the present case coupling effects are negligible. For the range of conditions herein the agreement between Eqn. 8a and 8b is better than 0.002 %. For definiteness, we calculate $C_{d,th}$ using Eqn. 8 b where $C_{d,1}$ is determined using the boundary layer model of Geropp for laminar flow and with the model of Stratford for turbulent flow, and $C_{d,2}$ is determined using the inviscid core model of Kliegel and Levine.

3. RESULTS

The measured discharge coefficients ($C_{d,exp}$) are graphically compared to theoretical values ($C_{d,th}$) over a Reynolds number range extending from 7.2×10^4 to 2.5×10^6. Strictly speaking, nine plots are necessary to account for the geometrical differences (*i.e.*, differing Ω) between the nine CFVs. However, instead of plotting nine graphs, we calculate $C_{d,th}$ using a single value of the curvature ratio (*i.e.*, $\Omega = 0.25$) for CFVs 1 through 7. This simplification allows a single plot for these seven CFVs while introducing only 0.023 % uncertainty in the predicted discharge coefficient. In contrast, CFVs 8 and 9 have curvature ratios that deviate significantly from $\Omega_{ISO} = 0.25$. For these CFVs, it was imperative to use the measured Ω. Separate plots were made for these two CFVs over their respective Reynolds number ranges.

Figure. 4 compares measured versus predicted values of discharge coefficient for CFVs 8 and 9. The figure shows the measured C_d data (◆) as well as two predicted C_d curves, one calculated with the measured Ω (▬) and the other using an assumed value $\Omega_{ISO} = 0.25$ (▬). For CFV 9, the difference between $C_{d,exp}$ and $C_{d,th}$ would be as much as 0.21 % (at the lowest Reynolds number) if we had assumed the CFV complied with ISO specifications with $\Omega_{ISO} = 0.25$. Similarly, for CFV 8 the difference would be 0.08 % if $C_{d,th}$ was calculated using $\Omega_{ISO} = 0.25$. In contrast, by using the measured Ω, the maximum differences are 0.065 % and 0.01 % for CFV 8 and 9, respectively.

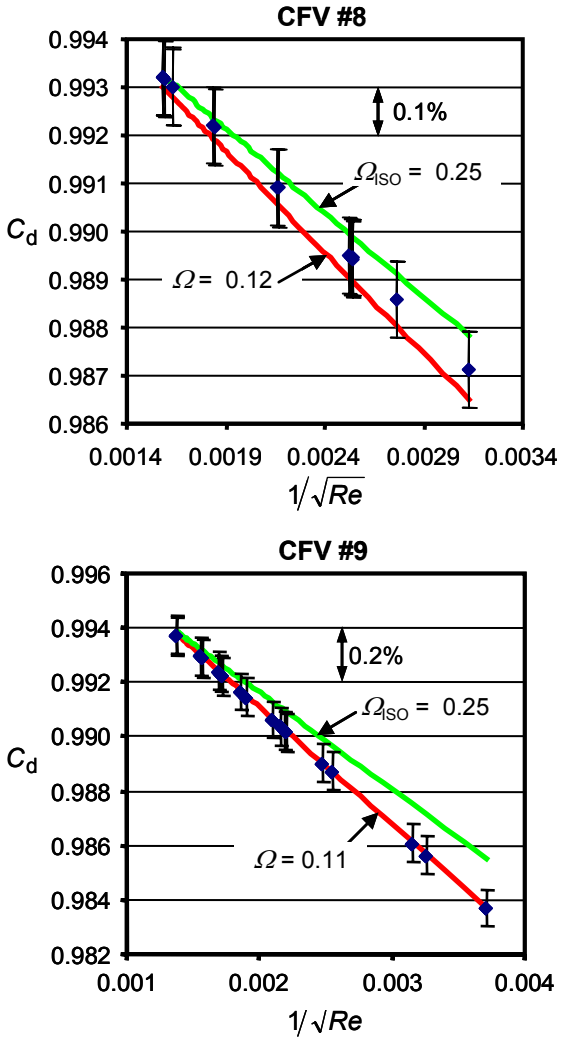

***Figure 4**. $C_{d,exp}$ versus $C_{d,th}$ for CFV 8 (top) and CFV 9 (bottom). ($C_{d,th}$ is calculated twice, once with the measured Ω and again using an assumed value $\Omega_{ISO} = 0.25$ consistent with ISO specifications.)*

Applying the measured value of the curvature ratio ($\Omega_8 = 0.12$) for CFV 8 did not yield a substantial improvement over $\Omega_{ISO} = 0.25$. Although not conclusive, we suspect that defects in the geometry of this CFV are responsible. In particular, the elliptically shaped cross section of this CFV resulted in a relative uncertainty of more than 50 % for Ω_8. If we hypothetically increased the throat curvature

[5] If virial effects are important than $C_{d,3}$ must be taken into account in these expressions.

ratio from 0.12 to 0.159 (*i.e.*, a 32.5 % increase), the agreement between theory and measurement would be better than 0.01 %. Nevertheless, the predicted $C_{d,th}$ using the measured Ω falls within the uncertainty bounds of the experimental data.

Figure 5 shows the measured C_d's for CFVs 1 through 7 plotted against a piecewise theoretical model that spans the laminar, transitional, and turbulent flow regimes. In the model, the transition to turbulence is assumed to occur at a single Reynolds number, $Re = 10^6$. The actual C_d data transitions from laminar to turbulent flow over a Reynolds number range extending from 1×10^6 to 2.1×10^6. At $Re < 10^6$ the data generally follows a linear trend typical of the laminar flow regime while for $Re > 2.1 \times 10^6$ the data appears to be fully turbulent and increases with increasing Reynolds number.

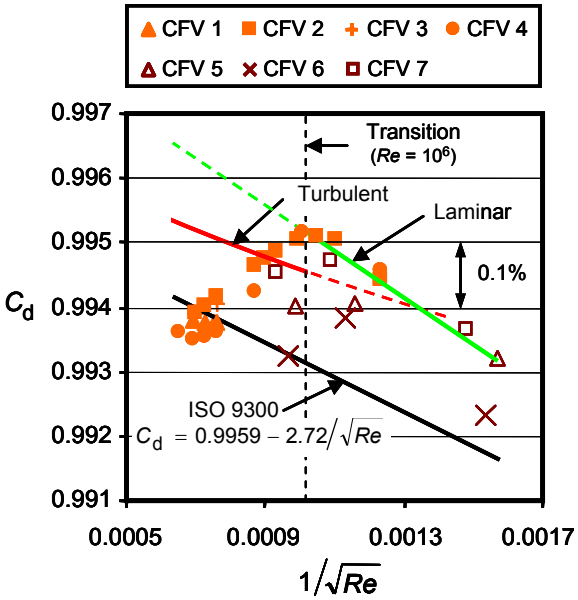

***Figure 5**. Measured discharge coefficient of CFVs 1 through 7 compared with the piecewise model spanning the laminar, transitional, and turbulent flow regimes.*

Excluding CFV 6 which had an uncertainty substantially larger than the other CFVs (refer to Table 1), the agreement in the laminar regime was better than 0.07 %. The worst agreement was in the turbulent regime where the predictive model overestimated the measured data by a nearly constant value of 0.14 %. The calibration data in the turbulent regime agreed better with the empirical C_d curve given by ISO [2].

4. CONCLUSIONS

Nine normally manufactured CFVs with nominal diameters ranging from 5 mm to 25 mm were calibrated in dry air, and their measured discharge coefficients agreed with predicted values to better than 0.17 % over a Reynolds number range extending from 7.2×10^4 to 2.5×10^6. For all nine CFVs the walls were smooth so that the effect of surface roughness was assumed negligible. The throat diameters (d) and the throat curvature ratio (Ω) of these CFVs were measured using a CMM. The theoretical discharge coefficient was determined by combining either Geropp's laminar boundary layer model [12] for $Re < 10^6$ or Stratford's turbulent boundary layer model [13] for $Re > 10^6$ with the inviscid core model of Kliegel and Levine [15].

The best agreement was found in the laminar regime where the difference between measured and predicted discharge coefficients was less 0.07 %. In contrast the turbulent model overpredicted the measured discharge coefficients by an almost constant offset of 0.14 %. Since the uncertainty of the measurements is also 0.14 %, more research should be done to determine if the bias is a result of the experimental measurements or the model.

The throat curvature ratio (Ω) played an important role for the two smallest CFVs. Dimensional measurements showed that the Ω of these CFVs significantly deviated from the intended ISO design value of $\Omega_{ISO} = 0.25$. When the predicted discharge coefficient was calculated using the measured values of Ω, the results were within the uncertainty of the calibration data. The smallest CFV exhibited the best results, agreeing with the experimental data to better than 0.01 %

The good agreement between measured and predicted C_d's gives credibility to using theoretical models to predict the discharge coefficient of geometrically well characterized CFVs. Additional research should be done to investigate what level of agreement can be achieved between measurement and theory in smaller CFVs where high accuracy dimensional measurements are more difficult, and differences between the boundary layer flow models of Tang [11] and Geropp [12] are more substantial.

REFERENCES

[1] Wright, J. D. *"The Long Term Calibration Stability Of Critical Flow Nozzles And Laminar Flowmeters"*, Proceedings of the 1998 NCSL Workshop and Symposium, Albuquerque, NM: NCSL, pp. 443-462, 1998.

[2] ISO 9300: (E), *"Measurement of Gas Flow by Means of Critical Flow Venturi Nozzles"*, Geneva Switzerland, 1990.

[3] Ishibashi, M., Takamoto, M., Watanabe, N., Nakao, Y. and Yokomizo, T., *"Precise Calibration of Critical Nozzles of Various Shapes at the Reynolds Number of 0.8 ~ 2.5 × 10^{5}",* Proceedings of Flow Measurement, Glasgow, U.K., 1994.

[4] Stoup, J. R., Doiron, T.D., *"The Accuracy and Versatility of the NIST M48 Coordinate Measuring Machine"*, SPIE Proceedings – Recent Developments in Traceable Dimensional Measurements, Vol 4401, pp 136-146, 2001.

[5] Wright, J. D., Johnson, A. N., and Moldover, M. M., *"Design and Uncertainty Analysis for a PVTt Gas Flow Standard"*, Journal of Research of the National Institute of Standards and Technology, Vol. 108, pp. 21-47, 2003.

[6] Johnson, A. N. and Wright, J. D., *"Gas Flowmeter Calibrations with the 26m^3 PVTt Standard"*, Journal of Research of the National Institute of Standards and Technology, in press.

[7] Johnson, A. N., Wright, J. D., Moldover, M. R., and Espina, P. I., *"Revised Uncertainty Analysis of the 26m^3 PVTt Flow Standard"*, Proceedings of 6th ISFFM Conference, Querétaro, Mexico., 2006.

[8] Johnson, A. N., Wright, J. D., Moldover, M. R., and Espina, P. I., *"Temperature Characterization in the Collection Tank of the NIST 26 m^3 PVTt Gas Flow Standard"*, Metrologia, Vol. 40, pp. 211-216, 2003.

[9] B. N. Taylor and C. E. Kuyatt, *"Guidelines for the Evaluating and Expressing the Uncertainty of NIST Measurement Results"*, NIST TN-1297, 1994.

[10] John, J. E., *"Gas Dynamics"*, Allyn and Bacon, Inc, 2nd edition, Boston, 1984.

[11] Tang, S., *"Discharge Coefficients for Critical Flow Nozzles and Their Dependence on Reynolds Numbers"*, Ph.D. Thesis, Princeton Univ., 1969.

[12] Geropp, D., *"Laminare Grenzschichten In Ebenen Und Rotationssymmetrischen Lavalduesen"*, Deutsche Luft- Und Raumfart, Forschungsbericht, pp. 71-90, 1971.

[13] Stratford, B. S., *"The Calculation of the Discharge Coefficient of Profiled Choked Nozzles and the Optimum Profile for Absolute Air Flow Measurement"*, Journal of Royal Aeron. Soc., Vol. 68, pp. 237-245, 1964.

[14] Hall, I. M., *"Transonic Flow in Two-Dimensional and Axially-Symmetric Nozzles"*, Quarterly Journal of Mechanics and Applied Mathematics, Vol. XV, Pt. 4, pp. 487-508, 1962.

[15] Kliegel J. R. and Levine J. N. *"Transonic Flow in Small Throat Radius of Curvature Nozzles",* AIAA Journal, Vol. 7, pp. 1375-1378, 1969.

[16] Johnson, R. C., *"Calculations of Real-Gas Effects in Flow Through Critical Nozzles",* Journal of Basic Engineering, pp. 519, 1964.

[17] Back, L. H., and Cuffel, R. F., *"Flow Coefficients for Supersonic Nozzles with Comparatively Small Radius of Curvature Throats"*, J. Spacecraft, Vol. 8, No. 2, pp. 196-198, 1971.

[18] Smith R. E. and Matz R. J., *"A Theoretical Method of Determining Discharge Coefficients for Venturis Operating at Critical Flow Conditions"*, J. Basic Eng., pp. 434-446, 1962.

[19] Massier, P., F., Back, L. H., Noel, M. B., and Saheli, F., *"Viscous Effects on the Flow Coefficient for a Supersonic Nozzle"*, AIAA Technical Note, pp. 605-607, 1970.

[20] Ishibashi, M., Takamoto, M., *"Very Accurate Analytical Calculation of the Discharge Coefficients of Critical Venturi Nozzles with Laminar Boundary Layer"*, Proceedings of the FLUCOME, Hayama, Japan, Sept. 14, 1997.

[21] White, F. M., *"Viscous Fluid Flow"*, McGraw-Hill, Inc., 1991.

[22] Johnson, A. N., Wright, J. D., Nakao, S., Merkle, C. L., Moldover, M. R., *"The Effect of Vibrational Relaxation on the Discharge Coefficient of Critical Flow Venturis"*, Flow

Measurement and Instrumentation, Vol. 11, Issue 4, pp. 315-327, 2000.

[23] Johnson, A. N., *"Numerical Characterization of the Discharge Coefficient in Critical Nozzles"*, Ph.D. Thesis, Pennsylvania State Univ., University Park, PA., Dec. 16, 2000.